The RFI 2022 Workshop at ECMWF, 14 - 18 February 2022
2022 URSI International Union of Radio Science

Characterization of the RFI Environment at the DRAO: The Classical Approach

Thushara Gunaratne*, Stephen Harrison, Timothy Robishaw and Brent Carlson
Dominion Radio Astrophysical Observatory (DRAO), Herzberg Astronomy and Astrophysics Research Centre,
National Research Council Canada, Penticton, British Columbia, Canada.

Abstract

The location of the Dominion Radio Astrophysical Observatory (DRAO) in interior British Columbia, Canada, was selected in part because of the expectation that the surrounding mountain ranges should shield the site against radio frequency interference (RFI) from terrestrial sources. In recent years, a number of radio telescopes have been hosted at DRAO. Since August 2021, the RFI novelty detection (RFInd) site monitor has been collecting data in order to characterize the RFI environment at DRAO and to exploit machine learning to identify hidden RFI signatures in the observations. The current configuration of the RFInd site monitor covers the frequency range from 350–1800 MHz for a single polarization with time resolution of 950 ms and frequency resolution of 3.33… kHz. The observations include hourly hot-cold calibration cycles. In the following we explain how classical methods have been used to process the collected RFI data and to analyze them with the objective of using the derived RFI information in the design of new radio astronomical instruments.

Index Terms— ARTTA-4, RFInd, site-characterization, spectrum-occupancy

1 Introduction

In spring/summer 1957, Jack Locke and Ed Argyle conducted a survey of several preselected sites in British Columbia in order to select a suitable site to host a radio telescope [1]. This survey identified the White Lake basin as the best location mainly due to the low RFI levels and large enough flat land for future antenna arrays but also due to the availability of amenities. It was expected that the surrounding mountain ranges (see Figure 1) would provide relatively good shielding against terrestrial RFI. In February 1959, the assembly of 26m Telescope (that was renamed the John A. Galt telescope in 2014) was commenced and the Dominion Radio Astrophysical Observatory (DRAO) was officially opened in summer 1960 [1]. Since then multiple radio telescopes including the Canadian Hydrogen Intensity Mapping Experiment (CHIME) and the DRAO Synthesis Telescope array have been hosted at DRAO to take advantage of the relative radio quietness and the available infrastructure [2]. Further, there have been several proposals to build new radio-telescopes/ instruments at DRAO [3].

Unfortunately, the RFI environment has been changing for the worse across the globe including at naturally shielded sites like DRAO. Ubiquitous use of wireless communication systems including mobile phones, smart-watches and automobiles equipped with vehicular radar have increased the number of RFI sources by orders of magnitudes over the past decades. Additionally, the deployment of *satellite mega-constellations* in recent years has posed a new set of challenges to earth-based optical and radio astronomy [4]. Therefore, the RFI environment at DRAO is of high interest for current and upcoming radio telescopes at the site.

The RFI novelty detection (RFInd) project at DRAO expects to characterize the RFI environment of the site and exploit machine learning to identify hidden RFI signatures in the observations [5]. The RFInd site monitor started collecting data in August 2021 amidst the challenges posed by the COVID-19 pandemic. Another ongoing project at DRAO is the Advanced Radio Telescope Test Array (ARTTA-4) with the aim of testing the "incoherent clocking" method [6] on the sky by upgrading the entire signal chains for four of the dishes in the existing Synthesis Telescope with state-of-the-art receiver, data-transmission, and digitizer technologies. Subsequently, this array will be used as a test bed for current and future technologies developed at DRAO and by its collaborators.

The front-end receiver system of ARTTA-4, in particular the digitizers, is being upgraded to alleviate data loss due to strong and impulsive RFI. A study has been initiated to estimate the achievable sensitivities with the ARTTA-4 and the RFI environment is a key factor in this estimation. In this study we expect to follow the classical approach [7] in characterizing the RFI environment at DRAO and we are particularly interested in the time variation of the *total RFI power* in the diurnal cycles. We hope that the agreement between the estimated and measured sensitivities would help us to come up with strategies to plan observations that could be extended to other larger radio telescopes such as the Square Kilometre Array Phase-1 (SKA1), next-generation Very Large Array (ngVLA), Atacama Large Millimeter and Sub-Millimeter Array (ALMA) and future radio telescopes.

2 The Signal Chain of the RFInd Site Monitor

The main signal conditioning/processing modules of the RFInd site monitor receiver system are shown in Figure 2. For the Alaris OMNI-A0190-4 receiver antenna, the horizontal beam pattern is omnidirectional and the vertical

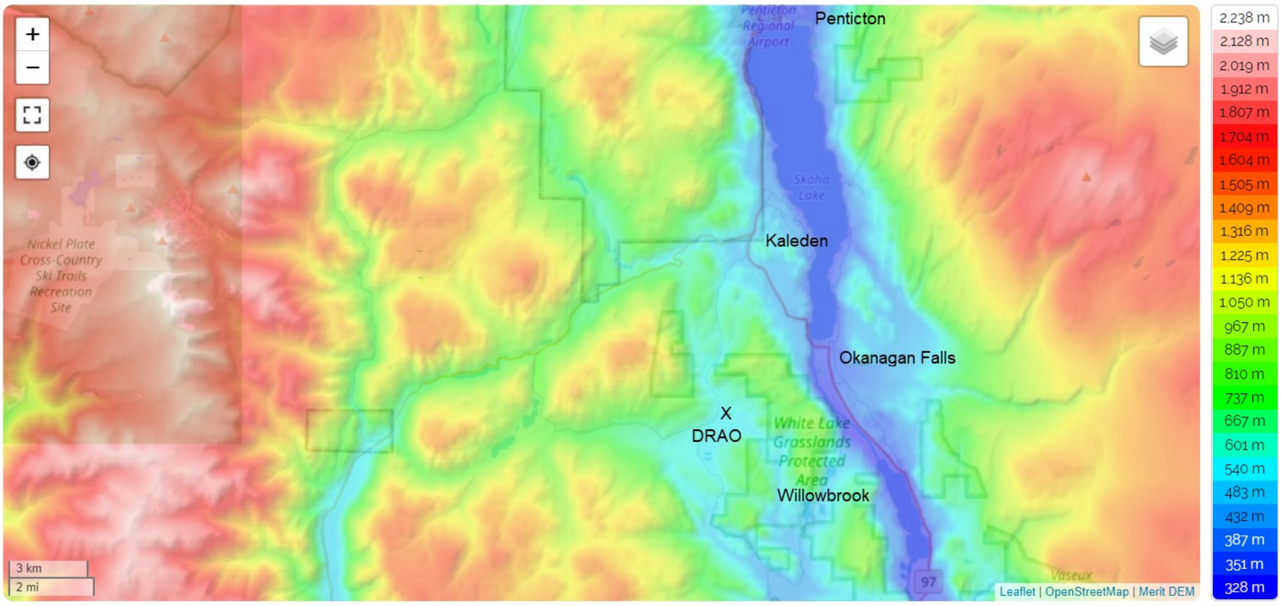

Figure 1. The topographical map of the South Okanagan region in interior British Columbia, Canada. The Dominion Radio Astrophysical Observatory (DRAO) is in close proximity to the communities of Willowbrook, Kaleden, Okanagan Falls and Penticton. As of 2022, the approximated populations in these communities are 300, 1,200, 2,500 and 39,000, respectively. (Source: https://en-ca.topographic-map.com/)

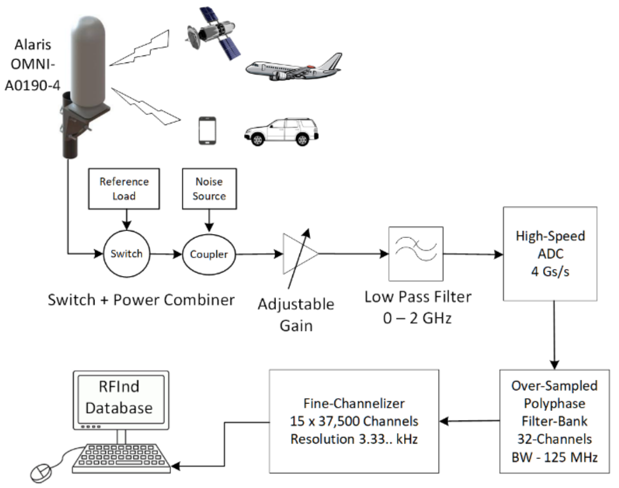

Figure 2. The main modules in the RFInd site monitor receiver systems.

beam pattern is dumbbell-shaped with 60° of nominal beamwidth. Hence, it is expected that the strength of skyborne RFI including from satellites is somewhat suppressed. The calibration signals from a 50 Ω matched load and a wideband noise source from Noisewave NW2G-30-CS with 30 dB excess noise ratio (ENR) are then combined with the antenna input using Mini-Circuit's MSP2T-18-12+ mechanical switch and ZGDC20-372HP+ directional coupler, respectively [8]. In combination the effective ENR into the RFInd receiver is ~10 dB.

The high-speed E2V 10AQ190 Analog-to-Digital Convertor (ADC) from Teledyne is configured to sample at 4 Gs/s, sampling the observing frequency band spanning 350–1850 MHz in the 1st Nyquist zone. The sampled sequence is processed by a 2-stage cascading channelizer arrangement. The first channelizer is an oversampling DFT polyphase filter-bank having the oversampling factor OS = 16/15 and yields 32 coarse channels containing 125 MHz of bandwidth. Next, 15 contiguous coarse channels corresponding to the one-sided spectrum spanning 0.0625–1.9375 GHz are processed by the critically-sampled polyphase DFT filter-banks segmenting each coarse channel into 40,000 fine channels where each fine channel is at the sample rate 3.33... kHz. Initially, the coefficients of the prototype filter for the critically-sampled fine channelizer were derived using the window-based method using a Hanning window function. The corresponding equivalent noise bandwidth of a fine channel was 0.7764. In November 2021, filter coefficients for the fine channelizer were replaced with new coefficients that were derived using an optimization method to achieve the equivalent noise bandwidth of 1.0.

Note that out of the total 15×40,000 = 600,000 fine channels generated by the critically-sampled filter-banks, there are 15×40,000/16 = 37,500 fine channels containing redundant spectral components and therefore, are discarded. The remaining 562,000 fine channels correspond to the one-sided spectrum spanning the observation bandwidth 0.0625–1.9375 GHz. A typical example of the recorded power in the 562,500 fine channels in the RFInd database at 03:04:07 on 2021-08-27 is shown in Figure 3. Because the data have not yet been calibrated the signal power is specified in ADC units. The total accumulated power across the 562,500 fine channels for each 950 ms accumulation in the hour 03:00 to 04.00 on 2021-08-27 is shown in Figure 4.

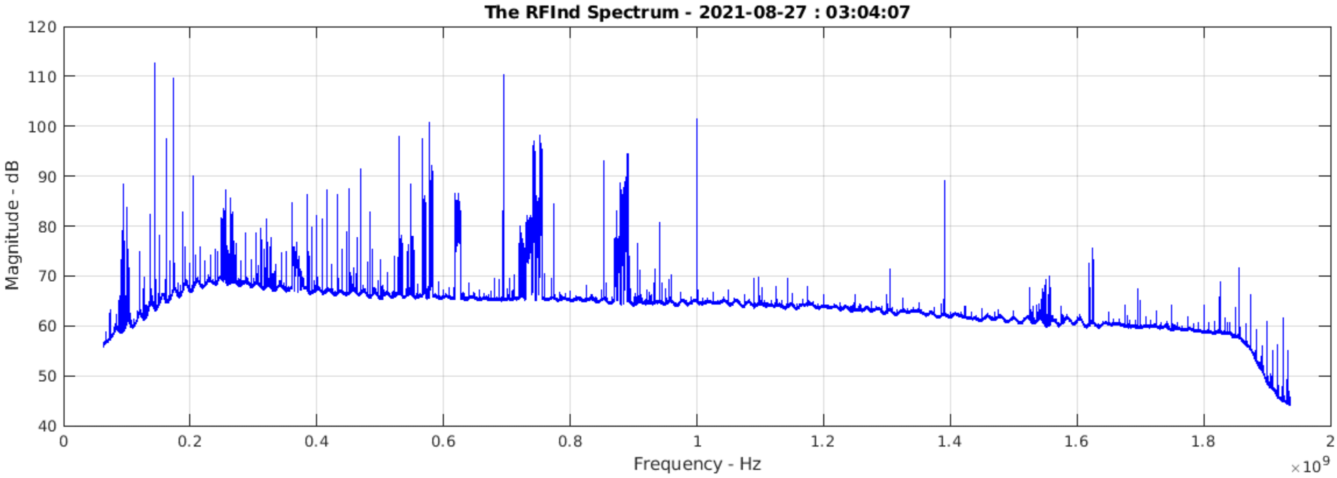

Figure 3. A typical record in the RFInd database containing the integrated power for 562,500 fine channels spanning the observation bandwidth 0.0625–1.9375 GHz. (In ADC units.)

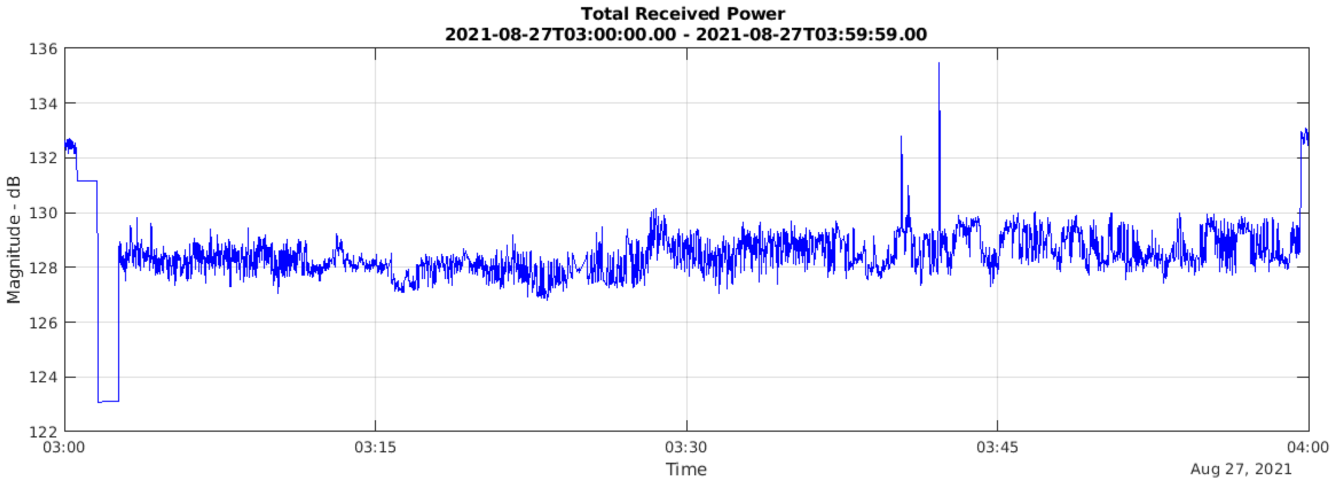

Figure 4. The total accumulated power across 562,500 fine channels for each integration in the RFInd database over a 1-hour interval. (In ADC units.)

3 Calibration of RFInd Data

The calibration cycle for the RFInd site monitor runs near the beginning of every hour with the following order:

1. 1 minute noise source + antenna
2. 1 minute noise source + matched load
3. 1 minute matched load only
4. 57 minutes antenna only

These calibration cycles can be seen in Figure 4.

The first step to estimate the RFI power spectral density is to determine the noise added by the front-end receiver system of RFInd. This is evaluated using the well-known Y-factor method, where the noise-figure $NF_{\mathrm{Rx}}(f_c)$ in dB at frequency f_c is given by,

$$NF_{\mathrm{Rx}}(f_c) = 10 \cdot \log_{10}\left(\frac{10^{\frac{\widetilde{ENF}}{10}}}{10^{\frac{Y(f_c)}{10}} - 1}\right), \qquad (1)$$

where $\widetilde{ENF}$ is the effective ENF = 10 dB and $Y(f_c)$ is the power difference in dB between calibration cycles 2 and 3. Note that the noise-factor measurement is accurate for the frequency range 250–1950 MHz where the RFInd receiver has sufficient gain. The measured noise-factor for the RFInd front-end receiver is shown in Figure 5. Note that mismatches in the ADC cause spectral artifacts at the sub-harmonics, e.g., 1 GHz, of the effective sampling rate 2 GHz. These channels are removed in the final analysis.

The receiver noise temperature, $T_{\mathrm{Rx}}(f_m)$, is given by

$$T_{\mathrm{Rx}}(f_m) = T_L\left(10^{\frac{NF_{\mathrm{Rx}}(f_c)}{10}} - 1\right), \qquad (2)$$

where $NF_{Rx}(f_m)$ is the estimated noise figure from (1). It is assumed that the matched load corresponds to constant noise temperature $T_L \approx 298$ K maintained in the shielded receiver box. The temperature inside the shielded box is also recorded near the beginning of each hour and stored in the RFInd database.

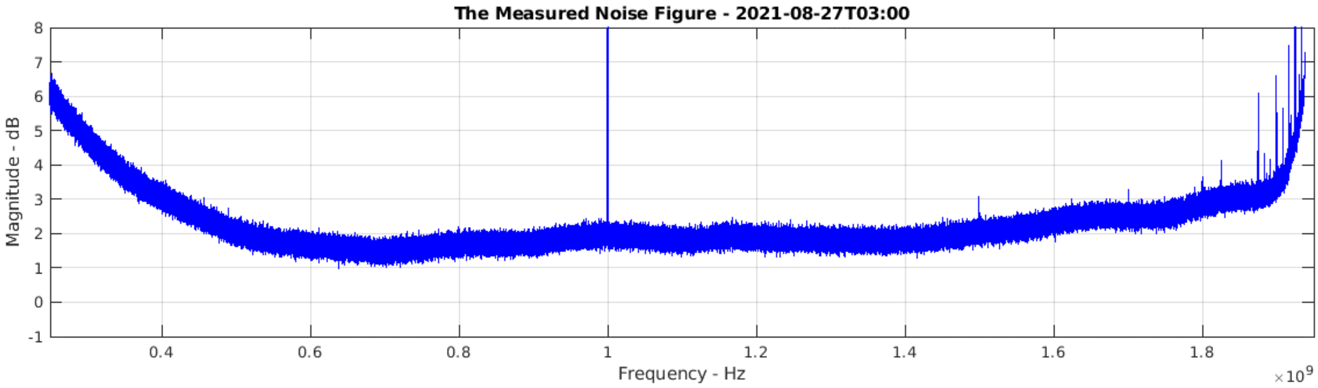

Figure 5. The measured noise figure for the RFInd front-end receiver.

Next, the gain $G_{\mathrm{Rx}}(f_c)$ of the RFInd receiver can be evaluated using the *Rayleigh-Jeans* approximation for thermal noise such that

$$G_{\mathrm{Rx}}(f_c) = \frac{P_{\mathrm{L}}(f_c)}{k\big(T_{\mathrm{L}} + T_{\mathrm{Rx}}(f_c)\big)BW}, \tag{3}$$

where $P_{\mathrm{L}}(f_c)$ is the noise power of the matching load in ADC units, k is the Boltzmann constant 1.3806485210^{-23} $\mathrm{m^2\,kg\,s^{-2}\,K^{-1}}$, and the effective bandwidth $BW = 0.7764 \times 3.33$ kHz. The power can be calculated as $P_{\mathrm{L}}(f_c) = E_{\mathrm{L}}(f_c)/\tau_{int}$, where $E_{\mathrm{L}}(f_c)$ the accumulated energy in ADC units and τ_{int} is the interval of integration.

Now, the integrated RFI power in ADC units, $P_{\mathrm{RFI}}(f_c)$, can be converted into the antenna temperature due to RFI with

$$T_{\mathrm{RFI}}(f_c) = \frac{P_{\mathrm{RFI}}(f_c)}{G_{\mathrm{Rx}}(f_c) \cdot k \cdot BW} - T_{\mathrm{Rx}}(f_c)\,. \tag{4}$$

Note that the minute contribution from the sky brightness and ground thermal noise is ignored in (4). The power spectral density of the RFI in dBm $\mathrm{Hz^{-1}}$ can be evaluated with

$$S_{\mathrm{RFI}}(f_c) = 10 \cdot \log_{10}(1000k \cdot T_{\mathrm{RFI}}(f_c))\,. \tag{5}$$

The estimate of the power spectral density for the frequency range 350–1850 MHz using the RFI measurement and the calibration made on 2021-08-27 at 03:57:51 is shown in Figure 6.

4 Evaluating the Basic Site-Characterization Parameters for ARTTA-4 Receivers

At DRAO, the ARTTA-4 project is underway to revitalize the receivers, signal chains and data-transport network for four of the dishes in the DRAO Synthesis Telescope array. The main objective of this project is to use the upgraded system to test and verify the "incoherent clocking" method [4] with on-sky data. As proposed in [5] the three basic site-characterization parameters are:

1. Total RFI power;
2. Interference-to-noise power ratio;
3. Time-frequency occupancy.

Here, the first two parameters of the above three are of interest and evaluated considering the two observing bands for ARTTA-4,

1. Band 1 : 400–800 MHz
2. Band 2 : 900–1800 MHz,

respectively. Given that the front-end receiver systems for both bands are still under development, an ideal 'brick-wall'-type transfer function is assumed for each receiver. Also, the receiver temperature is expected to be 50 K for both bands. According to [7, Figure 3], the sky brightness for Band 1 varies from 18 to 5 K and remains constant around 5 K for Band 2. It is estimated the average sky brightness for Band 1 is approximately 15 K. Given the above approximations, the system-noise estimates made using the *Rayleigh-Jeans* approximation for Bands 1 and 2 are given in Table 1.

In order to estimate the expected dynamic range of the signals received by the ARTTA-4 receivers, the RFI power distribution at the input to the ARTTA-4 receivers needs to be calculated for each band. Following ITU recommendation ITU-R RA.769-2, the antenna gain for the RFI signals has been selected to be 0 dBi. Hence, the signal power contained in fine channels within each band is aggregated to evaluate the total RFI power. Examples of the distribution of the total received power (i.e., RFI + system noise) with respect to the time for Band 1 and 2 made during the 22:00 hour on 2021-08-26 are shown in Figure 7 (a) and (b), respectively. The bin-width for each case is 0.118 dBm. Note that the RFI contribution from skyborne sources may be underestimated in RFInd measurements due to the antenna pattern of the site monitor.

Table 1. The Key Parameters of ARTTA-4 Receiver Systems

Parameter	Band 1	Band 2
Bandwidth - MHz	400	900
Receiver Noise Temp - K	50*	50*
Sky Brightness - K	15*	5
System Noise - dBm	-94.45*	-91.65*

*Expected values

As shown in Figure 8 the distribution of the expected received power for Band 1 is wider compared to that of Band 2. Therefore, the front-end receiver design for Band 1 has to facilitate the ~21.95 (i.e., 14.45+4.5+3) dB dynamic range with a 3 dB safety margin to maintain the linearity of the receiver 99% of the time [5]. Compared to this, the dynamic range requirement for Band 2 to achieve the same is ~ 11.65 (6.65+2+3) dB.

In order to achieve a given sensitivity η (e.g., 98%) at the correlator, the required *effective number of bits* (ENOBs) of the ADC for ARTTA-4 Bands 1 and 2 can be calculated as

$$ENOB = \log_2\left(\frac{CF \cdot RHR}{\sqrt{12 \cdot (1-\eta)}}\right), \tag{6}$$

where CF is the crest factor of the signal and RHR is the RFI headroom in linear scale [8]. Here, we have chosen the required receiver dynamic range as the RFI headroom. The crest factor is defined as the ratio of the peak amplitude to the rms level of the signal. Assuming $CF = 8$, in order to achieve sensitivity of 98%, the ADCs for ARTTA-4 Bands 1 and 2 need minimum ENOBs of 7.68 and 5.60, respectively.

5 CONCLUSIONS

Data collected with the RFInd site monitor at DRAO were used to extract classical RFI characteristics such as the total RFI power and the variation of total RFI power with time. Subsequently, these characteristics are used to determine the requirements for the signal chain design for the upcoming ARTTA-4 project. The RFInd measurements show that ARTTA-4 Band 1 (400–800 MHz) at DRAO is severely contaminated irrespective of the natural shielding provided by the surrounding mountain ranges. Although, the ARTTA-4 Band 2 (900–1800 MHz) seems relatively clear at the moment, the ubiquitous deployment of wideband wireless communication systems (e.g., 5G/6G), vehicular radar, and transmissions from satellite mega-constellations can directly or indirectly exacerbate the RFI contamination of the band. Therefore, effective regulations to limit RFI emissions and subsequent compliance monitoring are required to preserve the radio quietness at sites like DRAO. Further, advanced RFI mitigation techniques are needed at every stage of the signal processing to achieve the maximum possible sensitivity of radio telescopes.

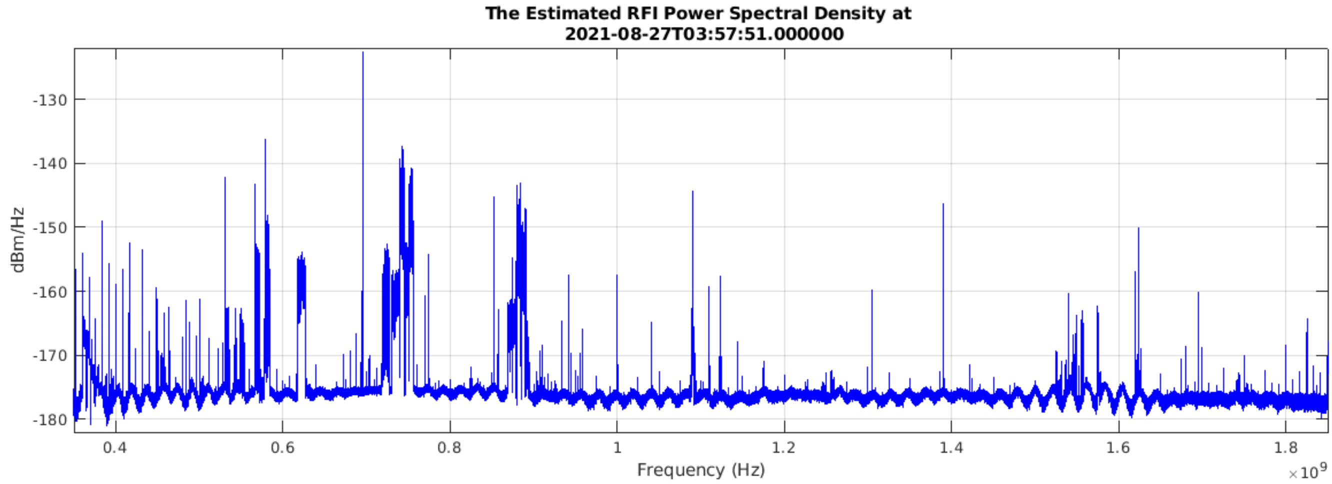

Figure 6. The estimate of the power spectral density of the RFI in the frequency range 350–1850 MHz on 2021-08-27 at 03:57:51.

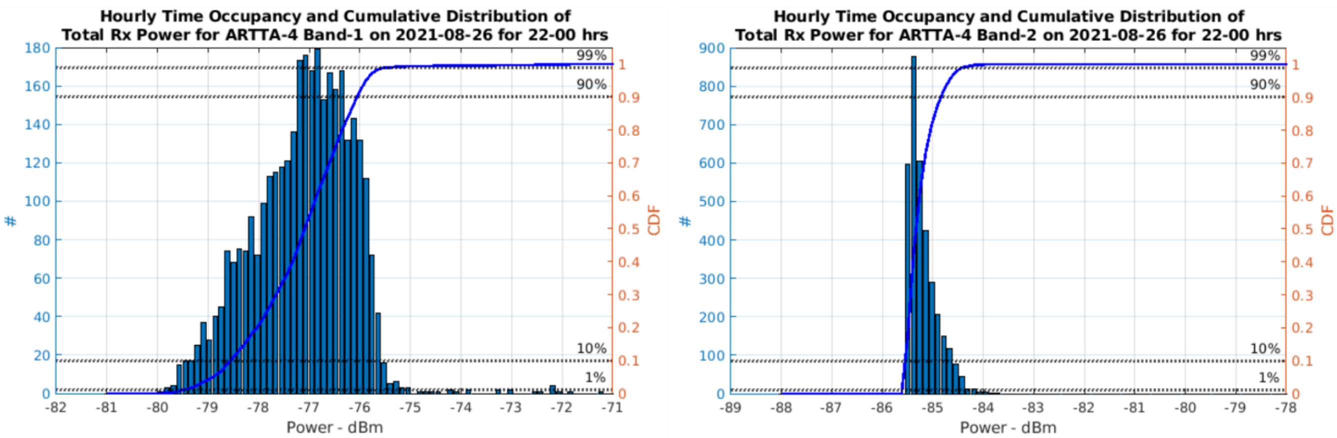

Figure 7. The expected distribution of total received power for ARTTA-4 Bands 1 and 2 for the 22:00 hour on 2021-08-26.

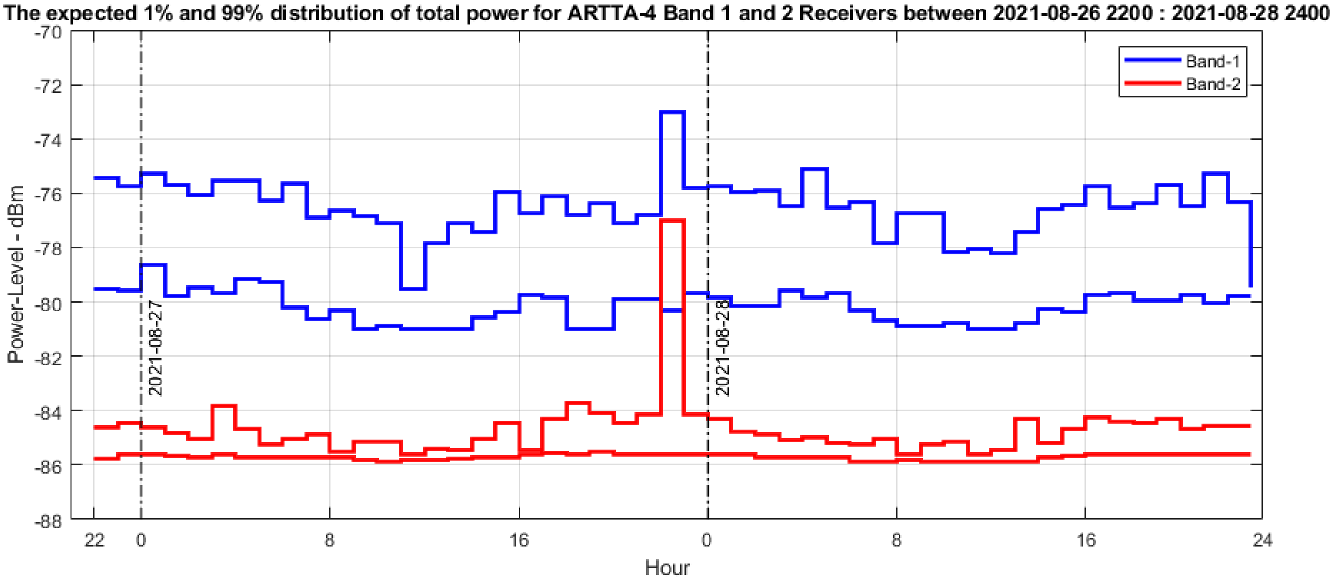

Figure 8. The expected 1% and 99% distributions of total power for ARTTA-4 Band 1 and 2 receivers from 2021-08-26 22:00 to 2021-08-28 23:00.

6. Acknowledgments

We would like to acknowledge support from our colleagues at DRAO who facilitated in commissioning, configuring and operating the RFInd site monitor during the challenging times due to the COVID-19 pandemic: in no particular order, C. Baard, M. Smith, R. Messing, B. Robert, R. Hellyer, D. Del Rizzo and D. Lagoy.

References

[1] J. Locke, "The Beginning of the Dominion Radio Astrophysical Observatory," Journal of the Royal Astronomical Society of Canada, vol. 92, p. 112, Jun. 1998.

[2] Dominion Radio Astrophysical Observatory research facility [online] https://nrc.canada.ca/en/research-development/nrc-facilities/dominion-radio-astrophysical-observatory-research-facility.

[3] Canadian Astronomical Society (CASCA), Canadian Astronomy Long Range Plan : 2022 – 2030. [online] https://casca.ca/wp-content/uploads/2021/04/20UOT001_CASCA_LRP_EN_vFA2.0.pdf.

[4] R. Massey, S. Lucatello, and P. Benvenuti, "The challenge of satellite megaconstellations", Nature Astronomy, 4, 1022–1023 (2020). https://doi.org/10.1038/s41550-020-01224-9S.

[5] Harrison et al., "RFI Monitor System Design for the Dominion Radio Astrophysical Observatory," in 2021 XXXIVth General Assembly and Scientific Symposium of the International Union of Radio Science (URSI GASS), Aug. 2021. doi: 10.23919/URSIGASS51995.2021.9560505.

[6] B. Carlson, "Incoherent clocking for radio telescopes", Proc. SPIE 11445, Ground-based and Airborne Telescopes VIII, 114458A (13 December 2020); doi: 10.1117/12.2562643.

[7] A. Chippendale and K. Wormnes, "Spectrum quietness metrics for radio astronomy," in 2013 Asia-Pacific Symposium on Electromagnetic Compatibility (APEMC), May 2013, pp. 1–4. doi: 10.1109/APEMC.2013.7360640.

[8] C. Baard, "RF Front-end Design Document (RFInd)", R1-DSN-000002 – Rev. A, 2019-11-20.

[9] G. C. Medellín, "Antenna Noise Temperature Calculation", Memo 95, 2007-07. [online] https://www.skatelescope.org/uploaded/6967_Memo_95.pdf.

[10] G. Comoretto, Private Communication, 2018-03-28.